A nomogram based on contrast-enhanced MRI and margin to identify lung metastasis in soft-tissue sarcoma

Yue Hu
China Medical University
Xiaoyu Wang
Cancer Hospital of China Medical University, Liaoning Cancer Hospital and Institute
Zhibin Yue
China Medical University
Hongbo Wang
Shengjing Hospital of China Medical University
Yan Wang
China Medical University
Yahong Luo
Cancer Hospital of China Medical University, Liaoning Cancer Hospital and Institute
Wenyan Jiang (xiaoya83921@163.com)
Cancer Hospital of China Medical University, Liaoning Cancer Hospital and Institute

Research Article

Keywords: soft-tissue sarcoma, lung metastasis, MRI, radiomics, nomogram

Posted Date: April 14th, 2022

DOI: https://doi.org/10.21203/rs.3.rs-1544374/v1

Abstract

Purpose

To develop a multi-modality MRI-based radiomics nomogram for predicting the lung metastasis (LM) in soft-tissue sarcoma (STS).

Methods

We enrolled 122 patients who clinicopathologically confirmed STS from our hospital to form a primary cohort. Thirty-two patients from another hospital were included as an external validation cohort. All patients underwent pretreatment T1-weighted contrast-enhanced (T1-CE) MRI scans. Radiomics features were calculated and selected from the T1-CE MRI sequence, and used to build the radiomics signature. Clinical factors were evaluated by the logistic regression. Multivariable logistic regression analysis was applied to construct a radiomics nomogram incorporating the radiomics signature with the important clinical factor. Receiver operating characteristic (ROC), calibration and decision curve analysis (DCA) curves were plotted to assess the radiomics methods.

Results

A total of 5 features were finally identified highly related to the LM status to develop the radiomics signature. A clinical-radiomics nomogram integrating the radiomics signature and margin achieved the best prediction performance in the training (AUCs, nomogram vs. radiomics signature vs. margin, 0.918 vs. 0.864 vs. 0.609), internal validation (AUCs, nomogram vs. radiomics signature vs. margin, 0.864 vs. 0.841 vs. 0.666) and external validation (AUCs, nomogram vs. radiomics signature vs. margin, 0.843 vs. 0.800 vs. 0.643) cohort. DCA indicated potential usefulness of the nomogram.

Conclusions

This study evaluated predictive values of T1-CE MRI for the prediction of lung metastasis in STSs, and proposed a nomogram model to potentially facilitate the preoperative individualized treatment decision making for STSs.

Introduction

Soft tissue sarcoma (STS) is a rare type of cancer arising from connective tissues and comprises more than 50 histologic subtypes (Nagar et al. 2018), with the 5-year overall survival rate approximately 50% (Schöffski et al. 2014). Distant metastasis has been considered as a poor prognostic factor in STSs, since the recurrence rate after resection is high (Deng et al. 2020). While, previous reports have shown a high distant metastasis rate of 30–40% in STSs, of which the lung metastasis is the most frequent site of metastasis and accounts for around 90% (Daw et al. 2015; Giuliano et al. 2016). Therefore, early and accurate detection of lung metastasis is crucial for making individual therapeutic decisions and improving prognosis in STSs.

In clinical practice, the fluoro-d-glucose (FDG) positron emission tomography (PET) and excisional biopsy are often required to assign a definitive diagnosis of lung metastasis in STSs. However, the FDG-PET has a relatively high rate of false positive results, and may not be affordable for some patients (Deng et al. 2020). Besides, the biopsy sampling requires significant expertise, and thus inappropriate biopsy may cause serious consequences and has been considered as a major error in the treatment of STSs (Frassica et al. 2000). Magnetic resonance imaging (MRI) is noninvasive and has been widely used as a routine diagnostic tool in oncology. While, MRI can hardly provide accurate information regarding the nature of the soft tissue mass (Demetri et al. 2005; Honoré et al. 2018). Since there are many subtypes of sarcomas that represent rarity and seemingly in the MRI image (Ezuddin et al. 2018), diagnoses based on MRI imaging features by visual-assessments are usually suspected (Hoang et al. 2018). Therefore, clinical evaluation of the soft-tissue masses is still limited by subjective experiences of clinicians (Chung et al. 2012). To our knowledge, there is still no specific MRI marker that has been evaluated for the preoperative prediction of lung metastasis in STSs.

In recent years, radiomics has been a rapidly growing discipline and considered as a promising and challenging field in cancer research, due to the capabilities of high-throughput analysis of quantitative features from medical images (Lambin et al. 2017). Numerous studies have highlighted values of radiomics in tumor diagnosis, prognosis and therapeutic response prediction (Kumar et al. 2012; Sollini et al. 2019). Radiomics has also been applied to reveal associations between MRI-based radiomics features and the underlying pathophysiology in soft-tissue masses. However, previous studies mainly focused on the differentiation of benign and malignant (Xu et al. 2014; Wang and Nie et al. 2020; Juntu et al. 2010), and prediction of histopathological grades (Wang and Chen et al. 2020; Zhang et al. 2019; Corino et al. 2018; Farhidzadeh et al. 2015) of the soft-tissue tumor. Recent efforts highlighted that some textural features from the FDG-PET (Deng et al. 2020) and T2 MRI (Vallières et al. 2015) image may be associated with the lung metastasis status in STSs. While, the studies had inherent bias with limited number of samples, which may be because of sample collection challenges since the STS is a rare disease with low incidence (Hoang et al. 2018). Inspired by the studies, we assumed that T1-

CE MRI-based radiomics may be predictive on the detection of lung metastasis in STSs, which to our knowledge has not been thoroughly studied. Thus, the goal of this study was to assess the predictive values of T1-CE MRI, and explore a clinical-radiomics nomogram and evaluate its potential clinical usefulness.

Materials And Methods

Patients

The retrospective study was approved by the institutional ethics committee of our hospital. In total, 122 consecutive patients from our hospital were enrolled to construct the primary group (mean age: 50; ranging from 19 to 82) and 32 patients from another hospital were included to construct the external validation group (mean age: 53.28; ranging from 28 to 75) between Jul. 2017 and Dec. 2021, according to the following inclusion criteria: (i) pathologically confirmed with lung metastasis, (ii) complete T1-CE MRI data before surgery, (iii) availability of clinical and pathological information, and (iv) older than 18 years. Exclusion criteria were: (i) with other tumor diseases, and (ii) received preoperative chemotherapy or radiotherapy. The patients were randomly divided into training and validation cohorts at a 2:1 ratio by stratified sampling. Baseline clinical characteristics, including age, gender, smoking, family history, past history, mobility, tenderness, hardness, size, margin, signal strength, T1 signal matrix and T2 signal matrix were obtained from medical records in our hospital. Table 1 lists histologic information of the enrolled patients.

Table 1
Summary of histologic types of the STSs enrolled in this study.

LM (n = 67)	Number	Non-LM (n = 87)	Number
Malignant fibrous histiocytomas	16	Malignant fibrous histiocytomas	20
Fibrosarcoma	6	Fibrosarcoma	9
Synovial sarcoma	3	Synovial sarcoma	5
Extraskelatal Ewing sarcoma	3	Extraskelatal Ewing sarcoma	4
Leiomyosarcoma	10	Leiomyosarcoma	11
Liposarcoma	10	Liposarcoma	13
Undifferentiated sarcoma	2	Undifferentiated sarcoma	4
Malignant tenosynovial giant cell tumor	1	Malignant tenosynovial giant cell tumor	1
Alveolar soft part sarcoma	1	Alveolar soft part sarcoma	3
Rhabdomyosarcoma	7	Rhabdomyosarcoma	11
Extraskeletal myxoid chondrosarcoma	1	Extraskeletal myxoid chondrosarcoma	2
Extraskeletal osteosarcoma	6	Extraskeletal osteosarcoma	3
Epithelioid sarcoma	1	Epithelioid sarcoma	1
LM: lung metastasis			

MRI protocol and Tumor segmentation

All patients were scanned using a 3T MR scanner (Verio, Siemens, Germany). The gadolinium-diethylenetriamine pentaacetic acid (Gd-DTPA) was used as the contrast agent for the T1-CE MRI scanning. The dose and speed of the Gd-DTPA injection were 0.1 mmol/kg and 3 ml/s, respectively. The parameters were: TR/TE = 700ms /11ms, FOV = 350mm×250mm, and matrix size = 256×256. For the MRI modality, a radiologist with 12 years' experience was invited to delineate the tumor alone the border in the MRI image to generate the region of interest (ROI) with the ITK-SNAP v.3.6 (url: www.itk-snap.org).

Radiomics feature extraction

For the T1-CE MRI sequence, a total of 1967 Features were calculated from the segmented ROIs with a "PyRadiomics" package as previously described (van Griethuysen et al. 2017). The features include three types: first-order, shape-based and textural features. The textural features characterized texture properties of the image region based on the gray-level size-zone matrix (GLSZM, n = 16), gray-level run-length matrix (GLRLM, n = 16), gray-level co-occurrence matrix (GLCM, n = 24), gray level dependence matrix (GLDM, n = 14), and neighborhood gray-tone difference matrix (NGTDM, n = 5). Transformations were performed on the original MRI images with eight different filters (localbinarypattern2D, laplacian of gaussian, square, wavelet, gradient, logarithm, exponential and squareroot) to generated filtered MRI images. Then, first-order and textural features

were calculated based on the filtered images to obtain high-dimensional features. Detailed descriptions of the radiomics features can be found in the Pyradiomics documentation (url: http://pyradiomics.readthedocs.io).

Feature selection

The intraclass correlation coefficient (ICC) analysis was performed with 30 randomly selected patients, fifteen were patients with LM and fifteen were patients without LM (Koo et al. 2016). Features with ICC > 0.85 were considered good consistency and retained. Next, the Mann-Whitney *U* test was applied to compare features between the LM and non-LM groups. Features with $P < 0.05$ were considered significantly and remained. Afterwards, the least absolute shrinkage and selection operator (LASSO) was applied to further select features with 10-fold cross-validation for the selection of optimal λ (Sauerbrei et al. 2007). At last, the most important features were identified with the logistic regression using the Akaike information criterion (AIC) (Pan 2001).

Development and evaluation of the radiomics models

The radiomics signature was developed based on the selected features weighted by their corresponding LASSO coefficients. The clinical-radiomics nomogram was constructed incorporating the radiomics signature and the important clinical parameter using the “rms” package in R language v.3.6. The ROC curve analysis was performed using the “pROC” package in R to evaluate the radiomics signature and compared with the Delong test. The paired t-test was used to determine the 95% confidence intervals. Calibration curves were plotted using the “rms” package to assess the goodness-of-fit of the nomogram. Decision curve analysis was performed using the “rmda” package to evaluate clinical utilities of the models by quantifying the net benefits of different threshold probabilities

Results

Clinical Characteristics

Table 2 listed statistical analysis results of the clinical characteristics. The margin was significantly different between the LM and non-LM groups in the training and internal validation cohort ($P < 0.05$). No significant difference was found between the LM and non-LM groups ($P > 0.05$) in regard to age, gender, smoking, family history, past history, mobility, tenderness, hardness, size, signal strength, T1 signal matrix, and T2 signal matrix.

Table 2
Clinical characteristics of the STS patients.

Characteristic	Training (n = 82)		*P*	Internal validation (n = 40)		*P*	External validation (n = 32)		*P*
	Non-LM (n = 47)	LM (n = 35)		Non-LM (n = 23)	LM (n = 17)		Non-LM (n = 17)	LM (n = 15)	
Age (Mean ± SD)	50.28 ± 14.91	51.45 ± 16.11	0.274	50.62 ± 13.30	51.94 ± 16.57	0.685	51.14 ± 15.72	54.13 ± 13.33	0.650
Sex (%)			0.745			0.289			0.266
Male	32 (68.1)	25 (71.4)		11 (47.8)	11 (64.7)		4 (23.5)	7 (46.7)	
Female	15 (31.9)	10 (28.6)		12 (52.2)	6 (35.3)		13 (76.5)	8 (53.3)	
Family history (%)			1.000			1.000			NA
Yes	4 (8.5)	2 (5.7)		1 (4.3)	0 (0.0)		0 (0.0)	0 (0.0)	
No	43 (91.5)	33 (94.3)		22 (95.7)	17 (100.0)		17 (100.0)	15 (100.0)	
Smoke history (%)			0.077			0.677			0.092
Yes	11 (23.4)	3 (8.6)		5 (21.7)	2 (11.8)		0 (0.0)	3 (20.0)	
No	36 (76.6)	32 (91.4)		18 (78.3)	15 (88.2)		17 (100.0)	12 (80.0)	
Past history (%)			0.634			0.471			0.513
Yes	34 (72.3)	24 (68.6)		16 (69.6)	14 (82.4)		6 (35.3)	7 (46.7)	
No	13 (27.7)	11 (31.4)		7 (30.4)	3 (17.6)		11 (64.7)	8 (53.3)	
Mobility (%)			0.563			0.730			0.291
Good	9 (19.1)	5 (14.3)		16 (69.6)	13 (76.5)		8 (47.1)	4 (26.7)	
Poor	38 (80.9)	30 (85.7)		7 (30.4)	4 (23.5)		9 (52.9)	11 (73.3)	
Tenderness (%)			0.844			1.000			0.265
Pain	34 (72.3)	26 (39.2)		17 (73.9)	12 (70.6)		8 (47.1)	10 (66.7)	
Non-pain	13 (38.3)	9 (60.8)		6 (26.1)	5 (29.4)		9 (52.9)	5 (33.3)	
Hardness (%)			0.943			0.683			0.529
Soft	5 (10.6)	3 (8.5)		1 (4.3)	0 (0.0)		0 (0.0)	0 (0.0)	
Tender	19 (40.4)	15 (42.9)		14 (60.9)	11 (64.7)		12 (70.6)	9 (60.0)	
Tough	23 (48.9)	17 (48.6)		8 (34.8)	6 (35.3)		5 (29.4)	6 (40.0)	
Size (%)			0.312			0.677			0.229
≥ 5cm	43 (91.5)	29 (82.9)		18 (78.3)	15 (88.2)		11 (64.7)	13 (86.7)	
< 5cm	4 (8.5)	6 (17.1)		5 (21.7)	2 (11.8)		6 (35.3)	2 (13.3)	
Margin (%)			0.027*			0.026*			0.088
Poor	30 (63.8)	30 (85.7)		14 (60.9)	16 (94.1)		11 (64.7)	14 (93.3)	
Well	17 (36.2)	5 (14.3)		9 (39.1)	1 (5.9)		6 (35.3)	1 (6.7)	
Signal strength			1.000			1.000			NA
Uniformity	1 (2.1)	1 (2.9)		1 (4.3)	0 (0.0)		NA	NA	
Non-uniformity	46 (97.9)	34 (97.1)		22 (95.7)	17 (100.0)		NA	NA	
T1 signal matrix			0.983			0.672			NA
Low	26 (55.3)	19 (54.3)		13 (56.5)	8 (47.1)		NA	NA	

LM: lung metastasis; SD, standard deviation; *, $p < 0.05$.

Characteristic	Training (n = 82)		P	Internal validation (n = 40)		P	External validation (n = 32)		P
	Non-LM (n = 47)	LM (n = 35)		Non-LM (n = 23)	LM (n = 17)		Non-LM (n = 17)	LM (n = 15)	
Mixed	18 (38.3)	14 (40.0)		8 (34.8)	6 (35.3)		NA	NA	
High	3 (6.4)	2 (5.7)		2 (8.7)	3 (17.6)		NA	NA	
T2 signal matrix			0.432			0.707			NA
Low	2 (4.3)	1 (2.9)		0 (0.0)	0 (0.0)		NA	NA	
Mixed	9 (19.1)	11 (31.4)		6 (26.1)	3 (17.6)		NA	NA	
High	36 (76.6)	23 (65.7)		17 (73.9)	14 (82.4)		NA	NA	
LM: lung metastasis; SD, standard deviation; *, $p < 0.05$.									

Feature selection and development of the radiomics signature

Figure 1 showed the selection of radiomics features with LASSO. A total of 5 features were finally identified as the most predictive features. The formula of radiomics signature was developed incorporating the 5 features weighted by their corresponding coefficients:

Radiomics signature = − 0.341 + 0.939 × lbp-3D-m2_glszm_ZoneEntropy − 0.627 × wavelet-LLL_glcm_MCC − 1.252 × original_shape_Sphericity − 1.462 × log-sigma-5-0-mm-3D_glszm_SmallAreaEmphasis + 1.309 × wavelet-LLL_firstorder_Minimum

Figure 2 depicted using the developed radiomics signature to predict LM. The results indicated that patients with or without LM can be roughly discriminated since the LM group generally exhibit higher radiomics signature values than the non-LM group. Table 3 listed prediction performance of each selected feature.

Table 3
Diagnostic performance of the selected features.

Feature	Cohort	Mean ± SD		AUC	P
		Non-LM	LM		
lbp-3D-m2_glszm_ZoneEntropy	Training	4.760 ± 0.449	5.108 ± 0.372	0.770	< 0.001
	Internal validation	4.752 ± 0.508	5.228 ± 0.268	0.777	0.002
	External validation	4.640 ± 0.505	5.109 ± 0.265	0.882	< 0.001
wavelet-LLL_glcm_MCC	Training	0.883 ± 0.066	0.841 ± 0.050	0.714	0.001
	Internal validation	0.868 ± 0.075	0.858 ± 0.043	0.535	0.725
	External validation	0.866 ± 0.057	0.803 ± 0.084	0.753	0.014
original_shape_Sphericity	Training	0.671 ± 0.074	0.578 ± 0.090	0.777	< 0.001
	Internal validation	0.663 ± 0.075	0.589 ± 0.068	0.772	0.003
	External validation	0.661 ± 0.057	0.592 ± 0.078	0.796	0.004
log-sigma-5-0-mm-3D_glszm_SmallAreaEmphasis	Training	0.530 ± 0.116	0.445 ± 0.129	0.656	0.016
	Internal validation	0.534 ± 0.138	0.463 ± 0.126	0.601	0.290
	External validation	0.263 ± 0.058	0.358 ± 0.122	0.698	0.058
wavelet-LLL_firstorder_Minimum	Training	-125.938 ± 108.322	-51.520 ± 160.727	0.658	0.015
	Internal validation	-58.968 ± 196.448	0.008 ± 191.230	0.624	0.191
	External validation	-118.253 ± 117.386	-125.001 ± 32.017	0.675	0.097
LM, Lung metastasis; AUC, Area under curve; SD, standard deviation.					

Construction and validation of the nomogram

The margin was identified as important independent clinical predictor. The radiomics signature and margin were integrated to construct the clinical-radiomics nomogram. As shown in Fig. 3(A), the nomogram model established with the radiomics signature in the second row, the margin in the third row, and the total points in the fourth row. Calibration curves showed good calibration of the nomogram-predicted and actual values (Fig. 3(B),

3(C) and 3(D)). ROC curves of each model were plotted and shown in Fig. 4. The nomogram exhibited the best predictive power with the highest AUC values. Table 4 compared predictive capabilities of the nomogram, radiomics signature and margin. The nomogram was superior to the radiomics signature in terms of AUC and ACC. The Delong test results revealed significant differences between margin and radiomics signature and between margin and nomogram.

Table 4
Comparisons of the radiomics signature, margin and nomogram model.

	Training					Internal validation					External validation				
	AUC (95% CI)	Acc	Spe	Sen	P	AUC (95% CI)	Acc	Sen	Sen	P	AUC (95% CI)	Acc	Sen	Sen	P
M1	0.609 (0.518–0.700)	0.573	0.638	0.857		0.666 (0.549–0.783)	0.575	0.609	0.941		0.643 (0.509–0.777)	0.531	0.353	0.933	
M2	0.894 (0.824–0.963)	0.817	0.894	0.771		0.841 (0.721–0.962)	0.750	0.783	0.765		0.800 (0.625–0.975)	0.531	0.824	0.867	
M3	0.918 (0.861–0.975)	0.841	0.936	0.771		0.864 (0.755–0.974)	0.750	0.652	0.941		0.843 (0.696–0.990)	0.625	0.882	0.800	
M1 vs. M2					< 0.001		0.032								0.182
M1 vs. M3					< 0.001		0.003								0.004
M2 vs. M3					0.0715		0.337								0.535

M1, Margin; M2, Radiomics signature; M3, Nomogram; AUC, Area under curve; CI, Confidence interval; Acc, Accuracy; Sen, Sensitive; Spe, Specificity.

Fig. 5 depicted DCA curves of the nomogram, radiomics signature and margin. The nomogram achieved the highest net benefit for the STSs among the three models when the threshold probability was between 0.09 and 0.94, which suggested good clinical potential of our proposed nomogram.

Discussion

Lung metastasis is a crucial factor leading to poor prognosis in STSs, but only limited studies have investigated values of preoperative imaging data on the prediction of lung metastasis (Deng et al. 2020; Vallières et al. 2015; Zhang and Ren 2020), mainly due to data collection challenges. In this study, we managed T1-CE MRI of STSs and evaluated the predictive values on the lung metastasis. A total of 1967 radiomics features were extracted and analyzed from the T1-CE MRI sequence, and 5 features were finally identified as the most predictive features associated with the lung metastasis. This was much more than a previous study related to our work that only evaluated 50 features in total (Vallières et al 2015). Among the selected features, there were 3 features belong to the textural feature category (glszm and glcm) and 1 feature belong to the shape-based feature category (shape). The glszm feature quantifies gray level zones in an image and the glcm feature maps the relationship between voxels within the region of interest, which reflect heterogeneity and gray level changes within the tumor. This may indicat that the intratumoral heterogeneity was highly associated with the lung metastasis in STS because textural features can characterize and quantify complexities across the region and often reflect tumor heterogeneities (Afshar et al. 2019). Our finding was partially in line with a recent study that also found textural features from FDG-PET were associated with the lung metastasis in STS (Deng et al. 2020). The original_shape_sphericity feature measures the roundness of the shape of the tumor region relative to a circle. The bigger this feature is, the rounder the tumor would be. Our findings revealed that the STSs represent more spherical shape tend to be without the lung metastasis, since the original_shape_sphericity feature values in the lung metastasis group were smaller than those in the non-lung metastasis group. This may be explainable considering the rounder tumors may have lower degrees of malignancy, and thus may have lower possibilities to metastasize.

We identified the margin as the most important clinical factor. Although there is no previous report described relationships between margin and lung metastasis in STS, a recent effort suggested the margin as a discriminative factor for the diagnosis of malignant soft-tissue tumor (Wang et al. 2020). This may be explainable since the margin reflect conditions of tumor edges which was highly associated with the degrees of malignancy, and hence related to the metastasis status. We found that when used alone, the margin generated lower AUC and ACC, but higher sensitivity compared with the radiomics signature. This may be because of the overestimation of the degree of malignancy of the STS by using margin alone,

due to the misjudging unclear peritumoral edema for the edges of the tumor. The Delong test revealed significant differences between the margin and radiomics signature, which indicates that the margin can provide complementary information to the imaging features. We found the age had no significant difference between the lung metastasis and non-lung metastasis groups ($P > 0.05$), which was inconsistent with a previous report that suggested age as an important clinical factor related to the lung metastasis in STSs (Deng et al. 2020).

When the margin was integrated with the radiomics signature, the constructed nomogram model can significantly improve the predictive performance, and generated AUCs ranging from 0.894 to 0.918, which was similar to those in a recent PET-based study for predicting the lung metastasis in STSs (Deng et al. 2020). Calibration curves showed good agreements between our nomogram-predicted and actual results. The DCA indicated that the nomogram can obtain more net benefit compared with the radiomics signature or margin. Therefore, we suggest the proposed nomogram can be considered as a potential tool for the prediction of lung metastasis in STSs.

The study has limitations. First, the sample size was relatively small, which was because the STS is a rare disease, and thus has sample collection challenges. While, multi-center studies with a larger sample size would be conducted in our future work. Second, a multi-modality study should be conducted since using CT/PET and MRI data combined with radiomics models may capture information from different modalities. Third, molecular data (e.g. genes and proteins) were not included, which should be evaluated and integrated to the radiomics models to generate better results. Fourth, deep learning-based radiomics was not investigated, which should be addressed to provide complementary information to the handcrafted feature-based radiomics.

Conclusions

This study evaluated values of T1-CE MRI-based radiomics for predicting the lung metastasis in STSs, and present a combined clinical-radiomics nomogram to potentially help clinicians guide the individual treatment decisions.

Declarations

Acknowledgements

The study was supported by Shenyang Municipal Science and Technology Project (F16-206-9-23), China National Natural Science Foundation (31770147), Project of Pneumoconiosis Prevention and Control of China's coal mines foundation (201909J033), National key research and development program (2017YFC0805208), and Medical-Engineering Joint Fund for Cancer Hospital of China Medical University and Dalian University of technology (LD202029).

Authors' contributions

HY: Conceptualization, Investigation, Data acquisition, Formal analysis, Methodology, Software, Visualization, Writing - original draft, Writing - editing; WX: Conceptualization, Data curation, Project administration, Formal analysis, Methodology, Writing – review; YZ: Data acquisition, Formal analysis, Methodology, Software, Writing – review; WH: Conceptualization, Data curation, Project administration; WY: Formal analysis, Methodology, Software; LY: Data curation, Project administration, Supervision; JW: Conceptualization, Project administration, Supervision, Validation, Writing - original draft, Writing – review. The author(s) read and approved the final manuscript

Availability of data and materials

The data used in this study is available from the corresponding author on reasonable request.

Code availability

The code used or analyzed during the current study are available from the corresponding author on reasonable request.

Ethics approval and consent to participate

All analyses of human data conducted in this study were approved by the Institutional Review Board of the Cancer Hospital of China Medical University and in accordance with the ethical standards of the institutional and/or national research committee and with the 1964 Helsinki declaration and its later amendments or comparable ethical standards. The need for informed consent was waived by the ethics committee of our hospitals in view of the retrospective nature of the analysis and the anonymity of the data

Conflict of interest

The authors have declared that no conflict of interest exists.

References

1. Afshar P, Mohammadi A, Plataniotis K N, et al (2019) From Hand-Crafted to Deep Learning-based Cancer Radiomics: Challenges and Opportunities. IEEE Signal Processing Magazine 4:132:160. https://doi.org/10.1109/MSP.2019.2900993.
2. Chung WJ, Chung HW, Shin MJ, et al (2012) MRI to differentiate benign from malignant soft-tissue tumours of the extremities: a simplified systematic imaging approach using depth, size and heterogeneity of signal intensity. Br J Radiol 85:e831-e836. https://doi.org/10.1259/bjr/27487871
3. Corino VDA, Montin E, Messina A, et al (2018) Radiomic analysis of soft tissues sarcomas can distinguish intermediate from high-grade lesions. J Magn Reson Imaging 47:829–840. https://doi.org/10.1002/jmri.25791
4. Daw NC, Chou AJ, Jaffe N, et al (2015) Recurrent osteosarcoma with a single pulmonary metastasis: a multi-institutional review. Br J Cancer 112:278–282. https://doi.org/10.1038/bjc.2014.585
5. Demetri GD, Baker LH, Beech D, et al (2005) Soft tissue sarcoma clinical practice guidelines in oncology. J Natl Compr Canc Netw 3:158–194.
6. Deng J, Zeng W, Shi Y, Kong W, Guo S (2020) Fusion of FDG-PET Image and Clinical Features for Prediction of Lung Metastasis in Soft Tissue Sarcomas. Comput Math Methods Med 2020:8153295. https://doi.org/10.1155/2020/8153295
7. Ezuddin NS, Pretell-Mazzini J, Yechieli RL, Kerr DA, Wilky BA, Subhawong TK (2018) Local recurrence of soft-tissue sarcoma: issues in imaging surveillance strategy. Skeletal Radiol 47:1595–1606. https://doi.org/10.1007/s00256-018-2965-x
8. Farhidzadeh H, Goldgof DB, Hall LO, et al (2015) Texture feature analysis to predict metastatic and necrotic soft tissue sarcomas. SMC 2798–2802. https://doi.org/ 10.1109/SMC.2015.488.
9. Frassica FJ, Khanna JA, McCarthy EF (2000) The role of MR imaging in soft tissue tumor evaluation: perspective of the orthopedic oncologist and musculoskeletal pathologist. Magn Reson Imaging Clin N Am 8:915–927.
10. Giuliano K, Sachs T, Montgomery E, et al (2016) Survival Following Lung Metastasectomy in Soft Tissue Sarcomas. Thorac Cardiovasc Surg 64:150–158. https://doi.org/10.1055/s-0035-1563538
11. Hoang NT, Acevedo LA, Mann MJ, Tolani B (2018) A review of soft-tissue sarcomas: translation of biological advances into treatment measures. Cancer Manag Res 10:1089–1114. https://doi.org/10.2147/CMAR.S159641
12. Honoré C, Faron M, Mir O, et al (2018) Management of locoregional recurrence after radical resection of a primary nonmetastatic retroperitoneal soft tissue sarcoma: The Gustave Roussy experience. J Surg Oncol 118:1318–1325. https://doi.org/10.1002/jso.25291
13. Juntu J, Sijbers J, De Backer S, Rajan J, Van Dyck D (2010) Machine learning study of several classifiers trained with texture analysis features to differentiate benign from malignant soft-tissue tumors in T1-MRI images. J Magn Reson Imaging 31:680–689. https://doi.org/10.1002/jmri.22095
14. Koo TK, Li MY (2016) A Guideline of Selecting and Reporting Intraclass Correlation Coefficients for Reliability Research. J Chiropr Med 15:155–163. https://doi.org/10.1016/j.jcm.2016.02.012
15. Kumar V, Gu Y, Basu S, et al (2012) Radiomics: the process and the challenges. Magn Reson Imaging 30:1234–1248. https://doi.org/10.1016/j.mri.2012.06.010
16. Lambin P, Leijenaar RTH, Deist TM, et al (2017) Radiomics: the bridge between medical imaging and personalized medicine. Nat Rev Clin Oncol 14:749–762. https://doi.org/10.1038/nrclinonc.2017.141
17. Nagar SP, Mytelka DS, Candrilli SD, et al (2018) Treatment Patterns and Survival among Adult Patients with Advanced Soft Tissue Sarcoma: A Retrospective Medical Record Review in the United Kingdom, Spain, Germany, and France. Sarcoma 2018:5467057. https://doi.org/10.1155/2018/5467057
18. Pan W (2001) Akaike's information criterion in generalized estimating equations. Biometrics 57:120–125. https://doi.org/10.1111/j.0006-341x.2001.00120.x
19. Sauerbrei W, Royston P, Binder H (2007) Selection of important variables and determination of functional form for continuous predictors in multivariable model building. Stat Med 26:5512–5528. https://doi.org/10.1002/sim.3148
20. Schöffski P, Cornillie J, Wozniak A, Li H, Hompes D (2014) Soft tissue sarcoma: an update on systemic treatment options for patients with advanced disease. Oncol Res Treat 37:355–362. https://doi.org/10.1159/000362631
21. Sollini M, Antunovic L, Chiti A, Kirienko M (2019) Towards clinical application of image mining: a systematic review on artificial intelligence and radiomics. Eur J Nucl Med Mol Imaging 46:2656–2672. https://doi.org/10.1007/s00259-019-04372-x
22. Vallières M, Freeman CR, Skamene SR, El Naqa I (2015) A radiomics model from joint FDG-PET and MRI texture features for the prediction of lung metastases in soft-tissue sarcomas of the extremities. Phys Med Biol 60:5471–5496. https://doi.org/10.1088/0031-9155/60/14/5471
23. van Griethuysen JJM, Fedorov A, Parmar C, et al (2017) Computational Radiomics System to Decode the Radiographic Phenotype. Cancer Res 77:e104-e107. https://doi.org/10.1158/0008-5472.CAN-17-0339
24. Wang H, Chen H, Duan S, Hao D, Liu J (2020) Radiomics and Machine Learning With Multiparametric Preoperative MRI May Accurately Predict the Histopathological Grades of Soft Tissue Sarcomas. J Magn Reson Imaging 51:791–797. https://doi.org/10.1002/jmri.26901
25. Wang H, Nie P, Wang Y, et al (2020) Radiomics nomogram for differentiating between benign and malignant soft-tissue masses of the extremities. J Magn Reson Imaging 51:155–163. https://doi.org/10.1002/jmri.26818

26. Xu R, Kido S, Suga K, et al (2014) Texture analysis on (18)F-FDG PET/CT images to differentiate malignant and benign bone and soft-tissue lesions. Ann Nucl Med 28:926–935. https://doi.org/10.1007/s12149-014-0895-9
27. Zhang L, Ren Z (2020) Comparison of CT and MRI images for the prediction of soft-tissue sarcoma grading and lung metastasis via a convolutional neural networks model. Clin Radiol 75:64–69. https://doi.org/10.1016/j.crad.2019.08.008
28. Zhang Y, Zhu Y, Shi X, et al (2019) Soft Tissue Sarcomas: Preoperative Predictive Histopathological Grading Based on Radiomics of MRI. Acad Radiol 26:1262–1268. https://doi.org/10.1016/j.acra.2018.09.025

Figures

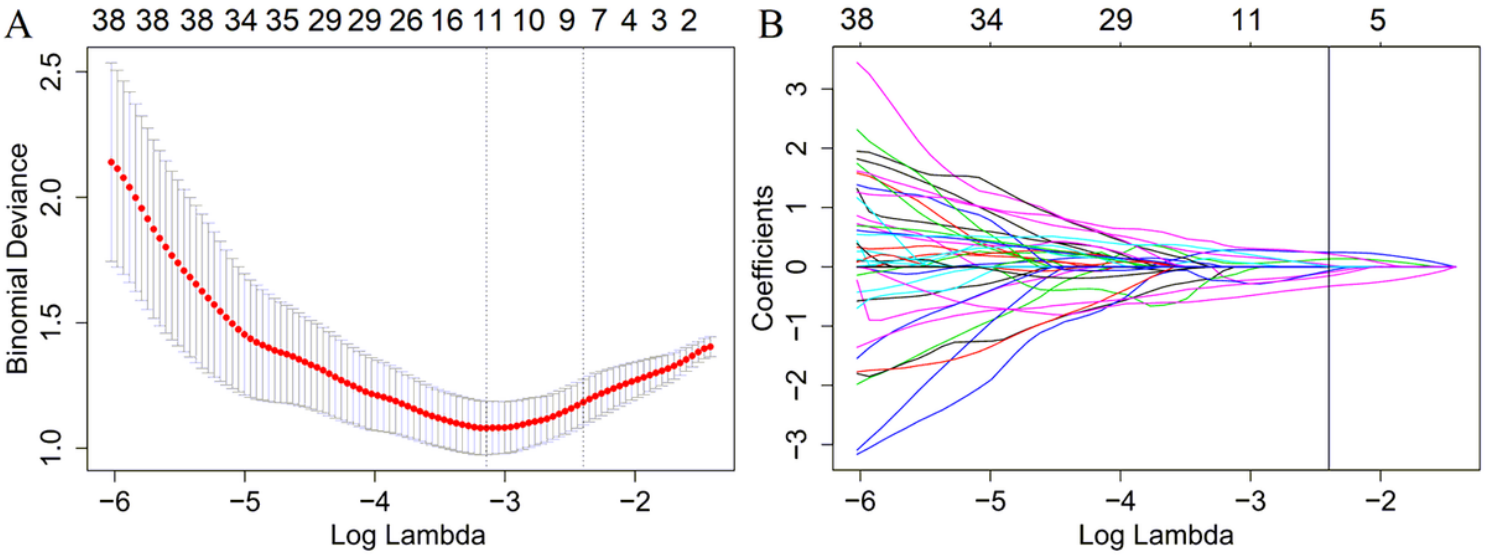

Figure 1

Feature selections from the T1-CE MRI with LASSO. (A) Tuning parameter Lambda selection in LASSO with 10-fold cross-validation. (B) LASSO coefficient profiles of the radiomics features, with 1-SE non-zero coefficients obtained from the MRI image.

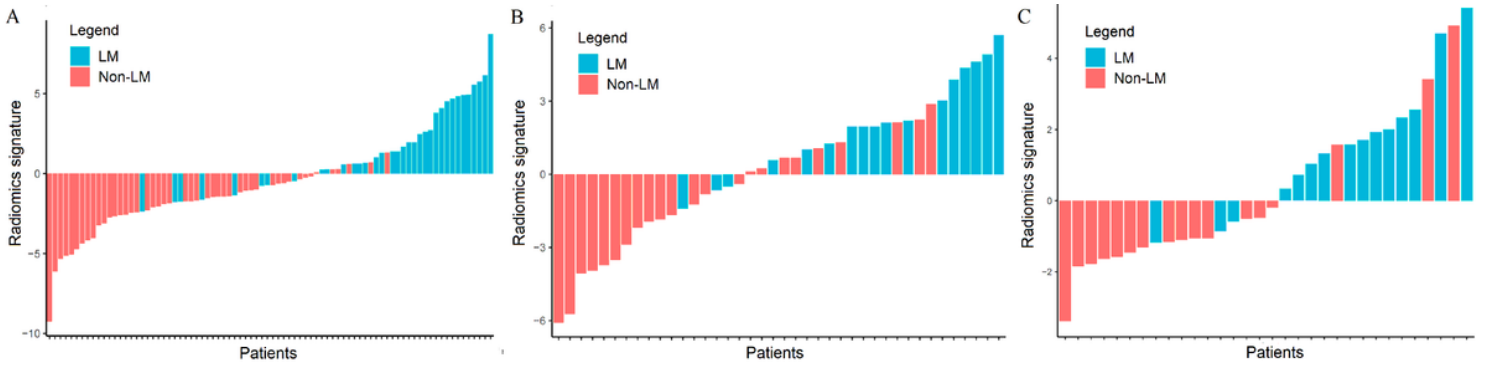

Figure 2

The radiomics signature for the STS patients in the training (A), internal validation (B) and external validation (C) cohort. The red bars represent the patients with LM, whereas the green bars indicate the patients without LM.

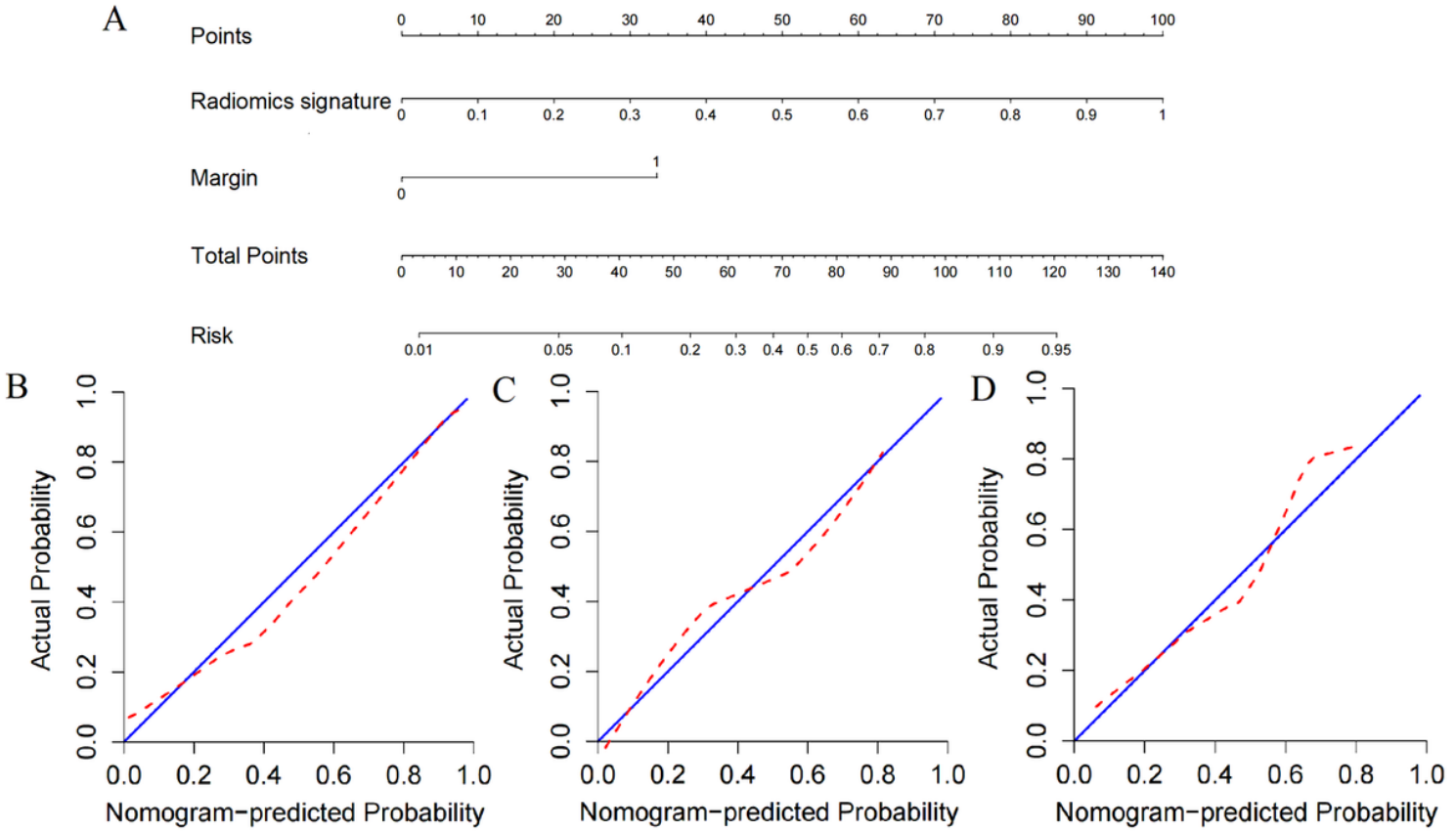

Figure 3

Construction and validation of the nomogram model. (A) The developed nomogram integrating the radiomics signature and margin. (B), (C) and (D) Calibration curves of the nomogram in the training (B), internal validation (C) and external validation (D) cohort.

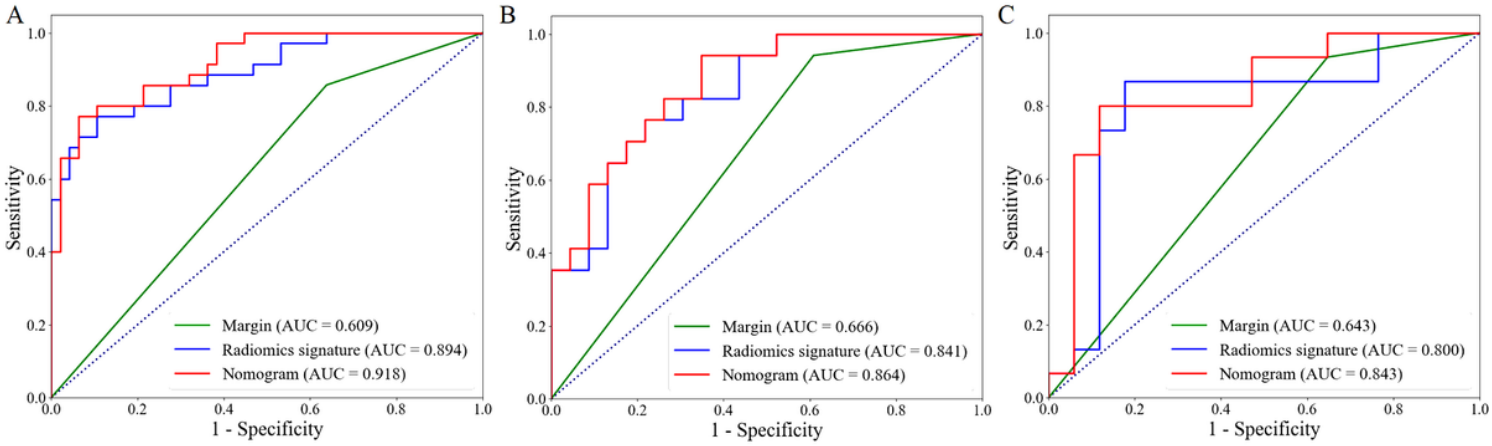

Figure 4

ROC curves of the margin, radiomics signature and nomogram in the training (A), internal validation (B) and external validation (C) cohort.

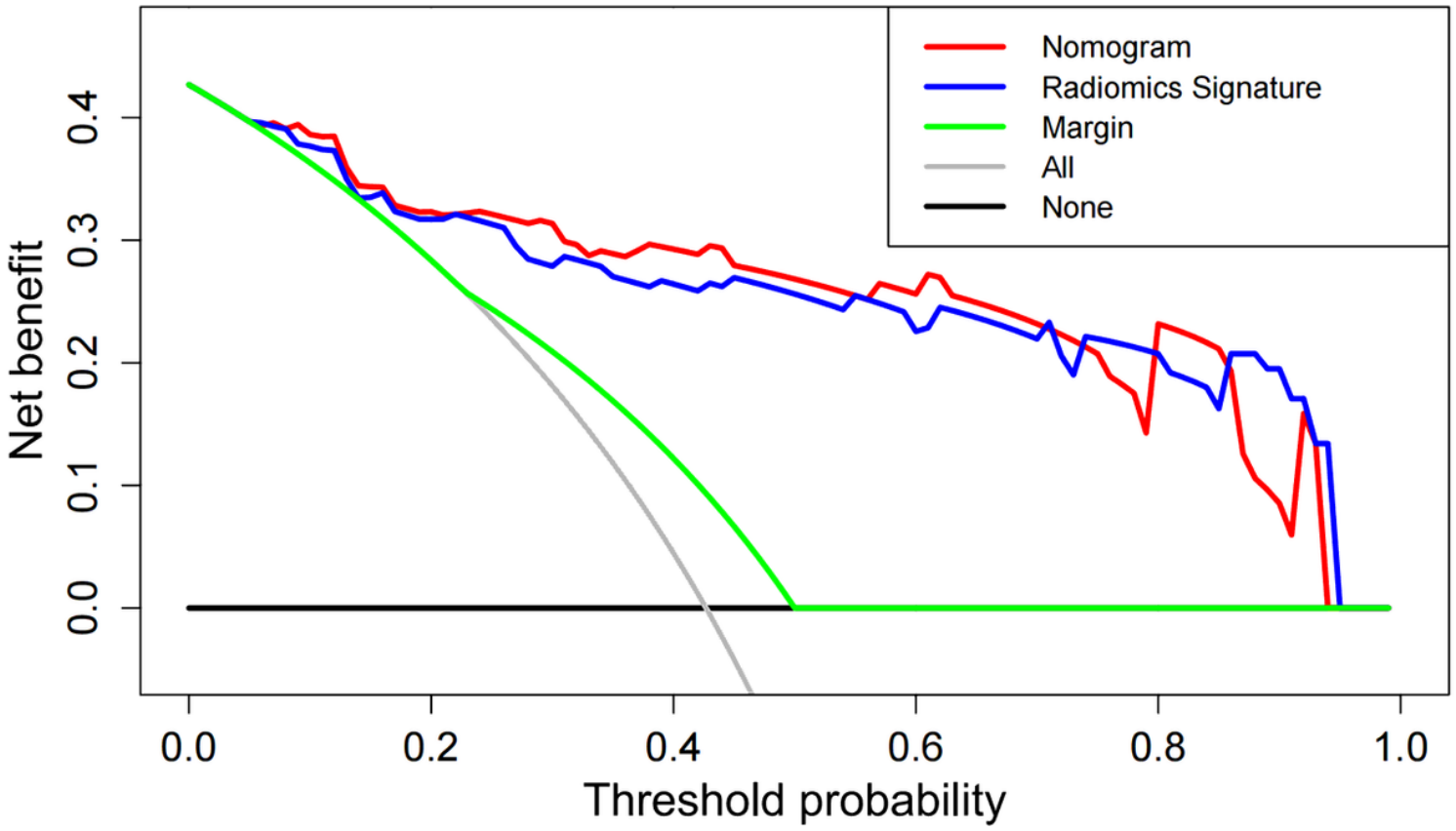

Figure 5

DCA curves of the radiomics signature, margin and nomogram. The x-axis represents the threshold probability, whereas the y-axis measures the net benefit for the patients. The black line represents the hypothesis that all patients were without LM. The gray line indicates the hypothesis that all patients were with LM. The red line represents the nomogram. The blue line represents the radiomics signature. The green line represents the margin.